
Graphical prediction of quantum interference-induced transmission nodes in functionalized organic molecules

Troels Markussen,^a Robert Stadler,^b and Kristian S. Thygesen^{*a}

Received Xth XXXXXXXXXXXX 2011, Accepted Xth XXXXXXXXXXXX 2011

First published on the web Xth XXXXXXXXXXXX 2011

DOI: 10.1039/b000000x

Quantum interference (QI) in molecular transport junctions can lead to dramatic reductions of the electron transmission at certain energies. In a recent work [Markussen *et al.*, *Nano Lett.* 2010, **10**, 4260] we showed how the presence of such transmission nodes near the Fermi energy can be predicted solely from the structure of a conjugated molecule when the energies of the atomic p_z orbitals do not vary too much. Here we relax the assumption of equal on-site energies and generalize the graphical scheme to molecules containing different atomic species. We use this diagrammatic scheme together with tight-binding and density functional theory calculations to investigate QI in linear molecular chains and aromatic molecules with different side groups. For the molecular chains we find a linear relation between the position of the transmission nodes and the side group π orbital energy. In contrast, the transmission functions of functionalized aromatic molecules generally display a rather complex nodal structure due to the interplay between molecular topology and the energy of the side group orbital.

1 Introduction

Quantum interference (QI) effects in molecular junctions has recently been suggested as an enabling tool for the implementation of molecular switches¹⁻³, logic gates⁴, data storage elements⁵ and thermoelectric devices⁶⁻⁸ in molecular electronics. These concepts originate from mesoscopics, where electron transport through waveguide devices has been investigated already two decades ago⁹⁻¹². In the context of single-molecule devices, QI were found to be responsible for the observed reduction of the conductance of a benzene contacted in the meta configuration as compared to the para and ortho configurations^{13,14}, and these findings were rationalized by a variety of different physical pictures, such as phase shifts of transmission channels or interfering spatial pathways¹⁵⁻¹⁸. More recently, the interest in QI has widened to aromatic molecules of increasing size¹⁹⁻²² and also to incoherent transport in the Coulomb blockade regime^{23,24}. One way to induce QI in molecular junctions is to control the electron transmission through chemical/conformational modification of side groups to aromatic molecules^{4,5,25-27}, but also simpler cross-conjugated molecular wires exhibit QI²⁸ and are promising candidates for implementing switching and rectifying behaviour²⁹.

Within the phase-coherent regime, electron transport through a molecular junction is described by the energy de-

pendent elastic transmission function, $T(E)$. In order to illustrate what is meant by QI in a molecular junction, it is instructive to consider the structure in $T(E)$ as arising from three distinct sources. First, we assume that the density of states in the electrodes is constant (wide band approximation) and that each molecular orbital contributes with an independent channel for electron transport. Under these simplifying assumptions, $T(E)$ is a sum of Lorentzian shaped peaks centered at the energy of the molecular orbitals (MOs). Next, we relax the wide band approximation. This will introduce additional structure in $T(E)$; in particular, the peaks in $T(E)$ will be shifted and change shape. Finally, we relax the assumption of independent transport channels. The structure introduced in $T(E)$ in this last step is referred to as a QI effect. The impact of QI on $T(E)$ depends on the relative energies and shape/symmetry of the MOs, and is in general difficult to predict. The most characteristic signature of QI is the presence of transmission nodes, i.e. destructive interference, in the energy gap between two adjacent MOs. For obvious reasons such transmission nodes are most interesting when they appear in the gap between the highest occupied molecular orbital (HOMO) and lowest unoccupied molecular orbital (LUMO) in which case the QI can suppress the conductance by several orders of magnitude.

In a recent work, we showed that the presence/absence of QI induced transmission nodes under certain conditions can be derived solely from the topological structure of the molecule using a very simple graphical method^{4,30}. In particular it was demonstrated that the graphical scheme correctly predicts QI interference in five out of ten different anthraquinone based

^a Center for Atomic-scale Materials Design (CAMD), Department of Physics, Technical University of Denmark, DK-2800 Kgs. Lyngby, Denmark; E-mail: trma@fysik.dtu.dk

^b Department of Physical Chemistry, University of Vienna, Sensengasse 8/7, A-1090 Vienna, Austria

structures. The graphical scheme is exact for a nearest neighbour tight-binding (TB) model with equal on-site energies, and therefore is expected to work well for all-carbon conjugated systems. The successful application of the scheme to systems containing heteroatoms, such as anthraquinone with its oxygen side groups, may seem surprising and calls for further analysis.

In this paper we relax the assumption of equal on-site energies. By doing so we can write down equations for the zero points of the transmission function directly from the graphs leading to a "generalized graphical scheme". For molecules, where the conjugated π system is defined by a linear carbon chain and a side group (which might contain heteroatoms), the scheme predicts a linear relationship between the energy of the QI induced transmission node and the energy of the π orbital of the side group. This behavior is confirmed by DFT calculations for molecules with a variety of different side groups. For aromatic molecules the situation is more complicated due to the interplay between topological and on-site energy effects. In general several QI induced minima occur in the transmission function; their energetic position is given by the roots of polynomials in energy which can be derived from the generalized QI graphs. We explore the dependence of these transmission nodes on the side group on-site energy for the ten anthraquinone structures of Ref.³⁰ using both TB and DFT calculations.

The paper is organized as follows. In Section 2 we summarize the graphical QI scheme from Ref.³⁰ and generalize it to the case of varying on-site energies (heteroatoms). More details on the graphical scheme are given in the Appendix. In Sections 3 and 4 we present our results for QI in functionalized molecular chains and aromatic molecules, respectively. The summary and conclusions are given in Section 5.

2 Graphical scheme

In this section we review our graphical approach to quantum interference. Some of the details in the derivation are further explained in Appendix A.

Within a single-particle picture, the transmission probability of an electron impinging on a molecular junction with an energy E is given by

$$T(E) = \text{Tr}[\mathbf{G}\mathbf{\Gamma}_L\mathbf{G}^\dagger\mathbf{\Gamma}_R](E) \quad (1)$$

where $\mathbf{G} = (E\mathbf{I} - \mathbf{H}_{\text{mol}} - \Sigma_L - \Sigma_R)^{-1}$ is the Green function matrix of the contacted molecule, \mathbf{I} is the identity matrix, $\Sigma_{L/R}$ is the self-energy due to the left/right lead, and $\mathbf{\Gamma}_{L/R} = i(\Sigma_{L/R} - \Sigma_{L/R}^\dagger)$. Let us assume that the Hamiltonian describing the molecule is given in terms of a basis consisting of localized atomic-like orbitals, $\phi_1, \phi_2, \dots, \phi_N$, and that only the two orbitals ϕ_1 and ϕ_N couple to the leads. In

this case the transmission reduces to

$$T(E) = \gamma(E)^2 |\mathbf{G}_{1N}(E)|^2. \quad (2)$$

Often the energy dependence on the lead coupling strength, γ , can be neglected. It then follows that the transport properties are entirely governed by the matrix element $\mathbf{G}_{1N}(E)$. The latter can be obtained using Cramer's rule

$$\mathbf{G}_{1N}(E) = \frac{C_{1N}(E\mathbf{I} - \mathbf{H}_{\text{mol}})}{\det(E - \mathbf{H}_{\text{mol}} - \Sigma_L - \Sigma_R)} \quad (3)$$

where $C_{1N}(E - \mathbf{H}_{\text{mol}})$ is the $(1N)$ co-factor of $(E\mathbf{I} - \mathbf{H}_{\text{mol}})$ defined as the determinant of the matrix obtained by removing the 1st row and N th column from $(E\mathbf{I} - \mathbf{H}_{\text{mol}} - \Sigma_L - \Sigma_R)$ and multiplying it by $(-1)^{1+N}$. Since we assume that only orbitals ϕ_1 and ϕ_N couple to the leads, the removal of the 1st row and N th column completely removes $\Sigma_{L,R}$ in the co-factor.

In the following we shall focus on $C_{1N}(E\mathbf{I} - \mathbf{H}_{\text{mol}})$ and represent the determinant graphically. We use the following notation: A hopping matrix element t_{ij} , $i \neq j$ is represented by a (red) line connecting site i and site j . For simplicity we restrict ourself to nearest neighbor hopping, but the application of the graphical scheme is not limited to this case. An on-site element $(\varepsilon_i - E)$ is represented by a (blue) *on-site loop*. Each on-site loop contributes a factor (-1) (see Appendix A). We shall set the on-site energy of the "back-bone" carbon atoms to zero, $\varepsilon_0 = 0$, but let the on site energy of any side groups, ε_{sg} , be of an arbitrary value. This is the main difference between this work and the previous work^{4,30}. Also, we will not limit the discussion to transmission at the Fermi energy, but consider transmission zeros throughout the energy range.

The generalized graphical scheme is summarized as follows: The transmission zeros can be determined from the zeros of the co-factor $C_{1,N}(E - \mathbf{H}_{\text{mol}})$. The terms in the co-factor can be represented graphically by drawing all possible diagrams according to the rules: (i) In each diagram the external sites connected to the electrodes must be connected to each other by a continuous path. (ii) All internal atomic sites must either have one ingoing *and* one outgoing path *or* have an on-site loop. (iii) The sign of a diagram is $(-1)^p$ where p is the total number of on-site loops and closed hopping loops. When we add up all diagrams constructed according to the above rules we obtain a polynomial in E whose roots represent the QI induced transmission nodes.

3 Simple molecular wires

We first apply our generalized graphical scheme to the simple system shown in Fig. 1 where the π system consists of a nine-atom carbon chain (C9) which is cross-conjugated with a side

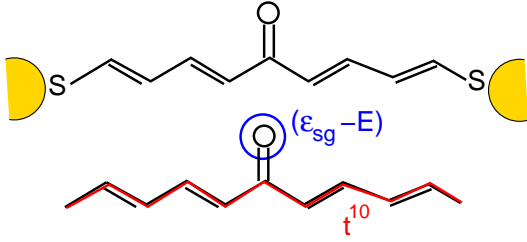


Fig. 1 Junction setup for a C9 chain with an oxygen side group (top). The generalized diagram is shown in the bottom.

group. Assuming nearest neighbor hopping there is only one possible path from left to right which invariably exhibits an on-site loop on the side group. This loop corresponds to a term $-(\varepsilon_{sg} - E)$ in the determinant of the cofactor, with ε_{sg} being the energy of the side group. The path from the left to right contacts consists of ten hoppings and thus contributes with a factor t^{10} , where t is the nearest neighbor hopping energy. To find the possible energies at which the transmission is zero, i.e. where $C_{1N}(\mathbf{H}_{\text{mol}} - E\mathbf{I}) = 0$, we have only one diagram to consider, which is shown in the bottom part of Fig. 1, and therefore must solve the trivial equation

$$-(\varepsilon_{sg} - E)t^{10} = 0 \Rightarrow E = \varepsilon_{sg}, \quad (4)$$

for the calculation of the energy, where the transmission zero in this case is equal to the on-site energy of the side group. We note that the energy of the transmission minimum is independent of the on-site energies of the carbon atoms in the chain and all hopping parameters in the molecule. Such a case where the energy dependence of the transmission minimum is linear with the side group energy will in the following be denoted as a simple side group transmission node. We note that such transmission nodes directly caused by the side group bears much resemblance with the general concept of a Fano resonance^{31,32} originating from the coupling of a localized state (the side group) with a continuum (extended states in the carbon chain). In Ref.³³ we have analyzed the analogy of the simple side-group transmission nodes with Fano resonances in more detail.

Figure 2 (left) shows the transmission for C9-type molecules as obtained from DFT calculations³⁴ with four different side groups: CH₂, O, NO₂, and CF₂. For all four molecules, we observe a distinct transmission minimum, where its energy can be tuned from $E - E_F = -1.4$ eV for O to $E - E_F = 1.7$ eV for NO₂. In order to illustrate the validity of the graphical scheme and the prediction from Eq. (4), we plot in the right panel of Fig. 2 the energy of the side group orbital ε_{sg} (see Appendix B for details) vs. the energy of the transmission minima E_0 . There is a clear linear dependence (with a slope of 1.2) in good qualitative agreement with Eq. (4). The deviation from a slope of 1 are probably due to

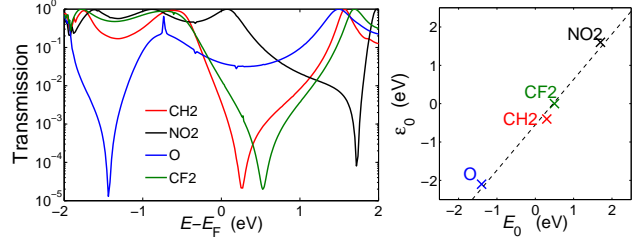


Fig. 2 Left: DFT calculated transmission functions for C9 with four different side groups. Right: π state eigenenergy of the side groups, ε_{sg} , plotted against the energy of the transmission minimum E_0 . The side group eigenenergy scales linearly with E_0 with a slope of ~ 1.2 .

the simplifying assumptions in the TB model of only nearest neighbour hopping, only a single p_z orbital on each atom, etc. In the DFT calculations there are interactions beyond nearest neighbours and several orbitals on each atom. In addition to this more subtle charge transfer effects may lead to deviations from the simple TB model. However, overall Eq. (4) gives a good description of the DFT data.

4 Aromatic molecules

We now consider the ten anthracene based molecules illustrated in Fig. 3, which only differ in the position of the two side groups. In Ref.³⁰ we studied the same molecules with oxygen side groups, then they become anthraquinones, and categorized them into two groups, where five of them exhibited QI in the HOMO-LUMO gap (I1-I5) and the others (N1-N5) did not. We made this distinction on the basis of our original graphical scheme and our conclusions were in good agreement with DFT calculations. This prediction, however, was based on the assumption that the on-site energy of the side group would be approximately equal to the on-site energy of the carbon p_z orbitals ($\varepsilon_0 \approx E_F$). From the side group analysis above, we see that this assumption is questionable for oxygen with a side group energy of $\varepsilon_O \approx -2$ eV (relative to the Fermi level). We note that this 2 eV difference in on-site energies should be considered relative to the size of the hopping matrix element which is ~ -3 eV. Still, the success we had in applying the graphical scheme^{4,30} to the anthraquinone molecules deserves a more careful analysis and explanation.

For this purpose we make use of a single-orbital nearest neighbour TB model with carbon on-site energies $\varepsilon_0 = 0$ and hopping elements $t = -2.9$ eV. We do not explicitly model the sulfur end group in the TB model, but include it as an effective part of the electrodes. Within this model we vary only the on-site energy of the side group and compute the transmission function within a wide band approximation, where the

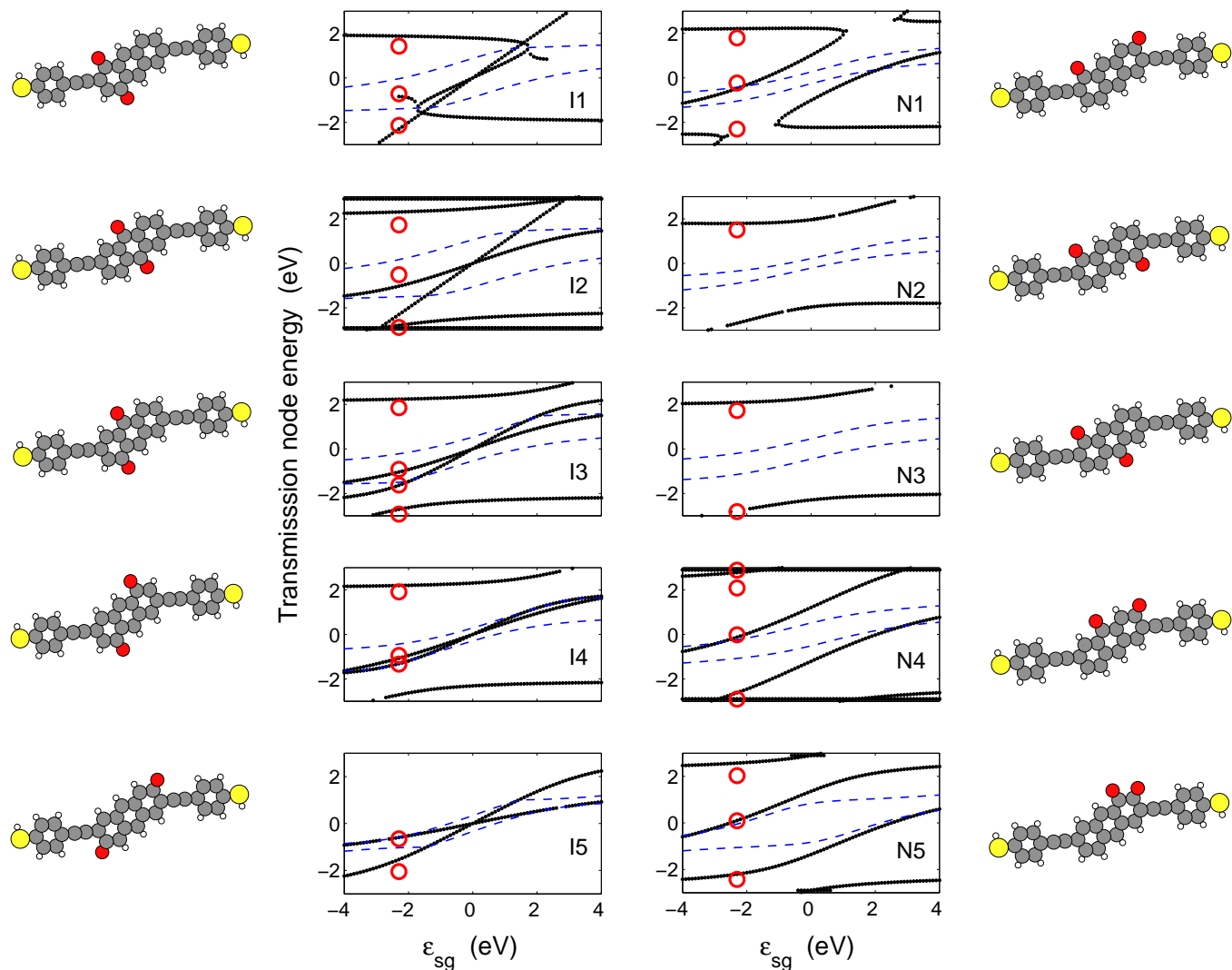


Fig. 3 Transmission node energies (black dots) for 10 different anthraquinone molecules as function of the side group on-site energy, ϵ_{sg} , as calculated in a nearest neighbour tight-binding model. The dashed curves show the HOMO (lower curve) and LUMO (upper curve) energies. The red circles are results from DFT calculations with oxygen side groups. Each panel in the two central columns corresponds to the molecular structure in the left- and right most columns. The molecules I1-I5 on the left side all exhibit QI in terms of transmission nodes within the HOMO-LUMO gap for most values of ϵ_{sg} , where no nodes are found in this energy range for any of the molecules N1-N5 on the right side for any realistic value of ϵ_{sg} .

results for the transmission zeros are shown in Fig. 3 as black dots. The lower and upper dashed lines show the energy of the HOMO and LUMO orbitals, respectively, while the red circles represent the results of DFT calculations with oxygen side groups³⁵. First, we note that the simple TB model is in excellent agreement with the DFT calculations, where both result in the same number and the same energetic positions of

transmission zeros. Our second observation is that the complexity of the dependence of the transmission minima on the on-site energy is quite striking, in particular when compared to the simple linear scaling found in the last section for the C9-type molecules.

In order to understand this complexity, we make use of the generalized graphical scheme introduced above. However, be-

fore turning to the anthraquinones we consider the related but simpler benzoquinone structure shown in the upper panel of Fig. 4. The lower panel shows the generalized diagrams. In addition to the displayed diagrams there are three additional but equivalent diagrams where the external sites are connected via the lower part of the molecule. These diagrams will simply contribute a factor of two to the resulting polynomials. As for C9 the on-site loops on the side groups again correspond to a term $-(\varepsilon_{sg} - E)$ in the determinant while for the carbon atoms we define $-(\varepsilon_0 - E) = E$ with $\varepsilon_0 = 0$.

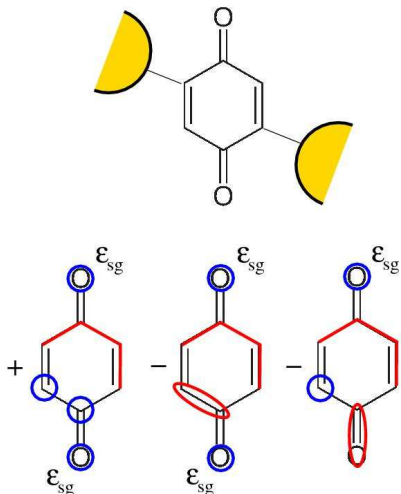


Fig. 4 Junction setup for a benzoquinone (top) and all the generalized diagrams (bottom).

Converting the diagrams into a polynomial and taking out their common factor $(\varepsilon_{sg} - E)t^3$, we arrive at the equation

$$(\varepsilon_{sg} - E)t^3 [E^2(\varepsilon_{sg} - E) - t^2(\varepsilon_{sg} - E) + t^2E] = 0, \quad (5)$$

which determines the transmission zeros. We note that it follows directly from the diagrams that there will be a maximum of four transmission nodes since there can be a maximum of four on-site loops no matter how the diagrams are drawn. The common factor in the equation corresponds to the common part of all three diagrams, where the upper oxygen on-site loop contributes $(\varepsilon_{sg} - E)$ and the path from left to right yields t^3 . We thus immediately see that for benzoquinone one of the transmission zeros is always at energy $E = \varepsilon_{sg}$, which is trivially defined by the side group on-site energy as for the C9 molecule in Fig. 1.

In addition to this simple side group transmission node, Eq. (5) has additional zeros defined by the third order equation

$$E^3 - \varepsilon_{sg}E^2 - 2t^2E + t^2\varepsilon_{sg} = 0. \quad (6)$$

While Eq. (6) can still be solved analytically, this results in rather lengthy expressions for the energies where $T = 0$ as

functions of ε_{sg} , which do not lend themselves to a transparent physical interpretation. Instead we solve the problem numerically and plot the results for all four transmission zeros in Fig. 5. The linear curve (black) corresponds to the simple side group transmission node at $E = \varepsilon_{sg}$. The remaining three zeros exhibit a more complicated behavior, where particularly the red curve is of interest because it is situated within the HOMO-LUMO gap (marked by the two dashed curves) for the whole range of ε_{sg} shown in Fig. 5. It is striking that although the benzoquinone is much simpler than the anthraquinone I2 (in terms of the total number of atoms), the nodal structures of the two corresponding transmission functions are very similar. Most importantly, this applies for both, the simple side group transmission node (black curve in Fig. 5) and the minimum which is situated within the HOMO-LUMO gap (red curve in Fig. 5). Also the remaining two transmission nodes below the HOMO and above the LUMO are similar for I2 and benzoquinone.

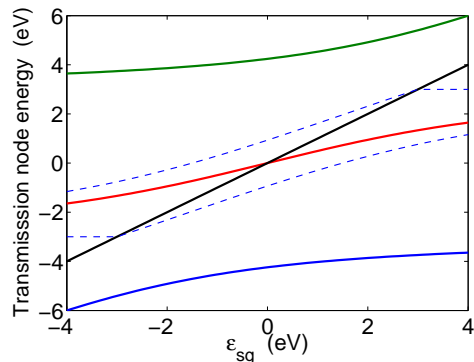


Fig. 5 Energy of transmission nodes E_i for the benzoquinone as function of side group on-site energy, ε_{sg} . The dashed lines mark the HOMO (lower line) and LUMO (upper line) of the molecule. While the simple side group transmission node (black) falls outside the HOMO-LUMO gap for large values of $|\varepsilon_{sg}|$, another node (red curve) stays in the HOMO-LUMO gap for all values of ε_{sg} .

From the five molecules with transmission zeros inside the HOMO-LUMO gap, I1-I5, only I1 and I2 have a simple side group transmission node. This is straightforward to explain by using our generalized graphical scheme. I1 and I2 are characterized by having both side groups on the same benzene ring, and therefore every path from the left to the right contact has to go through at least one carbon atom with a side group directly attached. This means that all valid diagrams have at least one on-site loop, where $(\varepsilon_{sg} - E)$ becomes a common factor among them, resulting in a simple side group transmission node. For I3-I5 on the other hand, it is possible to draw valid diagrams with no on-site loop on a side group, which we illustrate in Fig. 6 (top) with a diagram for the central part of

I3. If such a diagram is possible, no common factors can be found for all diagrams, and hence no simple on-site transmission node exists. The nodal spectra of the transmission functions for I3-I5 thus has to be solely defined by higher order polynomial equations which we find indeed in Fig. 3.

We note that all the structures I1-I5 have transmission zeros within the HOMO-LUMO gap up to rather large side group on-site energies $|\varepsilon_{sg}| \lesssim 2.0$ eV. These are the molecules expected to show QI based on the predictions from our original graphical scheme^{4,30}. This is consistent with the underlying assumption of that scheme, namely that the variation in on-site energies should be smaller than the hopping matrix element which is ~ 3 eV in the present case.

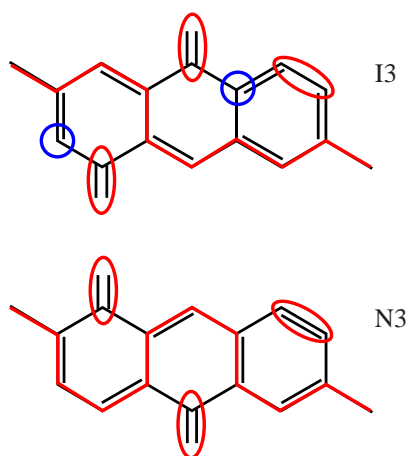


Fig. 6 Examples of diagrams for I3 (top) and N3 (bottom). I3 will always have on-site loops (blue circles), but not necessarily on the side group. The N3-diagram has no on-site loop and contributes with a finite value at all energies.

We now turn our attention to the five molecules N1-N5, which we previously predicted not to have transmission zeros in the relevant energy range around the Fermi energy³⁰. Strictly speaking our predictions on the basis of the simpler graphical scheme in Ref.³⁰ were limited to the assessment of the absence or occurrence of transmission zeros at the Fermi level, when $\varepsilon_{sg} = 0$. From the data plotted in Fig. 3 we can now confirm that even allowing for a rather large variation of the side group on-site energies, namely for $|\varepsilon_{sg}| \lesssim 2.5$ eV, there are indeed no transmission zeros to be found within the HOMO-LUMO gap. We now show how the simple graphical scheme of Ref.³⁰ is a special case of the generalized graphical scheme we introduce in the current paper. When $\varepsilon_{sg} = \varepsilon_0 = 0$, all diagrams containing on-site loops will be zero, which implies for the I1-I5 molecules that all diagrams deliver zero terms to the polynomial equations and the transmission is zero at $E = 0$. Since there are always two on-

site loops, as shown in Fig. 6 (top), the transmission node at $E = 0$ eV for $\varepsilon_{sg} = 0$ will be doubly degenerate. By changing ε_{sg} the degenerate nodes split into two and node crossings are observed for all I1-I5. For the molecules N1-N5 there are, however, always diagrams without on-site loops (an example is shown for N3 in Fig 6 (bottom)) which will thus contribute a finite value to the transmission at $E = 0$.

We conclude that the categorization of the ten anthraquinone molecules into interfering (I1-I5) and non-interfering (N1-N5) predicted by the simple graphical scheme of Ref.³⁰ holds for all realistic values of ε_{sg} . Only for very large values of $|\varepsilon_{sg}|$, which would require side groups which do not couple to the aromatic π system and are therefore irrelevant for our considerations here, deviations can occur. Fig. 3 shows for instance that I1 has no transmission nodes in the HOMO-LUMO gap for $|\varepsilon_{sg}| \gtrsim 2.5$ eV, while for N1 a transmission node enters the HOMO-LUMO gap for equally rather large $|\varepsilon_{sg}|$ values.

5 Conclusions

We have discussed how characteristic quantum interference (QI) induced nodes in the transmission function of conjugated molecules can be predicted from simple graphical considerations involving only the topology of the molecule and the on-site energy of non-carbon elements of the π -system. A previously introduced diagrammatic scheme, strictly valid for all-carbon molecules, was shown to be qualitatively valid for molecules containing different atomic species as long as the on-site energies (p_z -orbital energies) do not vary too much compared to the interatomic hopping strength – a condition we found to be met for a range of conjugated molecules with different side groups (O, CH₂, NO₂, CF₂). We showed that more quantitative estimates of the transmission node position can be obtained from a straightforward generalization of the graphical scheme to the case of finite (and varying) on-site energies. This scheme was then used to analyze the transmission nodes in linear and aromatic molecules with side groups. For linear molecular chains a single transmission node occurs at an energy corresponding to the energy of the side group π -orbital while for aromatic molecules the nodal structure of the transmission function is in general more complex due to a non-trivial interplay between molecular topology and side group on site energy. The richness of the nodal structure provides a flexible design tool for applications of QI in electronic devices based on molecular junctions.

Acknowledgement TM and KST acknowledge support from FTP grant nr. 274-08-0408 and The Danish Center for Scientific Computing. The center for Atomic-scale Materials Design (CAMD) is supported by the Lundbeck Foundation. RS is currently supported by the Austrian Science Fund FWF, projects Nr. P20267 and Nr. P22548.

A Derivation of the generalized graphical scheme

We shall illustrate the derivation of the graphical scheme by considering the four site ‘‘molecule’’ shown in Fig. 7 (top). The molecule is connected to the contacts at site 1 and site 4. The Hamiltonian describing the molecule is

$$\mathbf{H}_{\text{mol}} = \begin{pmatrix} \varepsilon_1 & t_{12} & 0 & t_{14} \\ t_{21} & \varepsilon_2 & t_{23} & 0 \\ 0 & t_{32} & \varepsilon_3 & t_{34} \\ t_{41} & 0 & t_{43} & \varepsilon_4 \end{pmatrix}. \quad (7)$$

As shown in Section 2, transmission zeros are determined by the zeros of the co-factor $C_{1N}(E - \mathbf{H}_{\text{mol}})$. The relevant co-factor for the four-site molecule is

$$C_{14}(E - \mathbf{H}_{\text{mol}}) = \begin{vmatrix} -t_{21} & E - \varepsilon_2 & -t_{23} \\ 0 & -t_{32} & E - \varepsilon_3 \\ -t_{41} & 0 & -t_{43} \end{vmatrix}. \quad (8)$$

The evaluation of the determinant can be done using Laplace’s formula,

$$\det(A) = \sum_{j=1}^n A_{i,j}(-1)^{i+j} M_{i,j}, \quad (9)$$

where the minor $M_{i,j}$, is the determinant of the matrix that results from A by removing the i -th row and the j -th column (i.e. the cofactor without the sign). Since the on-site energies appears in the first upper diagonal at indices $(i, i + 1)$, each factor $(E - \varepsilon_i)$ have a sign factor $(-1)^{2i+1} = -1$, and thus contribute with a minus sign. In the minor $M_{i,i+1}$ the on-site terms will still be in the first upper diagonal and thus contribute with an additional minus sign.

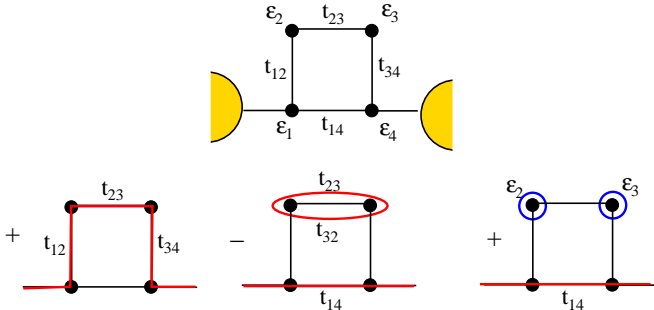


Fig. 7 Top: Four site molecule connected to electrodes at site 1 and 4. Bottom: All the diagrams determining the transmission zeros.

Writing down the elements of the co-factor gives an equation for the transmission zeros (the minus sign is included for notational simplicity):

$$\begin{aligned} -C_{1N}(E - \mathbf{H}_{\text{mol}}) &= 0 \\ t_{12}t_{23}t_{34} - t_{14}t_{23}t_{32} + (\varepsilon_2 - E)t_{14}(\varepsilon_3 - E) &= 0. \end{aligned}$$

The three terms in the co-factor can be represented graphically with the following convention: Each hopping element t_{ij} is drawn as a line from site i to site j . Note that in all diagrams, the terminating sites (in this case site 1 and 4) are connected by a continuous path of hopping elements. An on-site term $(\varepsilon_i - E)$ is drawn as a circle around site i and contributes a factor (-1) . We also note that the loop $t_{23}t_{32}$ going back and forth between site 2 and 3 in the middlemost diagram gives a minus sign. It is a general rule, that closed loops, similar to on-site loops, contributes a minus sign. This can also be derived from Laplace’s formula: A hopping element t_{ij} appears at index $(i - 1, j)$ in the co-factor determinant, Eq. (8). By evaluation of the co-factor along the $(i - 1)$ ’th row the terms involving t_{ij} will contribute with a sign $(-1)^{i-1+j}$. The new minor appearing after removing the $(i - 1)$ ’th row and j ’th column will have the hopping element t_{ji} at index $(j - 2, i)$, assuming without loss of generality that $i > j$. In evaluating this minor along the j ’th column, the term t_{ji} comes with a sign $(-1)^{j-2+i}$ and the over all sign of the combination $t_{ij}t_{ji}$ is $(-1)^{2i+2j-3} = -1$. This shows that a loop between two neighbouring sites contributes a minus sign. The over all sign of a diagram is thus $(-1)^p$ where p is the total number of on-site loops and neighbour loops.

In summary, the transmission zeros can be determined from the zeros of the co-factor $C_{1N}(E - \mathbf{H}_{\text{mol}})$. The terms in the co-factor can be represented graphically by drawing all possible diagrams according to the rules: (i) In each diagram the terminal sites connected to the electrodes must be connected to each other by a continuous path. (ii) A path can be drawn between sites i and j having non-zero hopping elements, t_{ij} . It is not limited to nearest neighbour interactions only. (iii) All remaining, internal sites must either have one ingoing *and* one outgoing path *or* have an on-site loop. (iv) The sign of a diagram is $(-1)^p$ where p is the total number of on-site loops and closed hopping loops.

B Computation of on-site energies

We calculate the side group on-site energy from the full Hamiltonian matrix, \mathbf{H} , describing the molecule and the Au electrodes. We project onto the subspace spanned by the basis functions of the side groups:

$$\mathbf{h}_{sg} = \mathbf{P}_{sg} \mathbf{H} \mathbf{P}_{sg},$$

where \mathbf{P}_{sg} has diagonal elements on the indices of the side group basis functions, and zeros elsewhere. Similarly we get a side group overlap matrix, \mathbf{s}_{sg} . We then diagonalize $\mathbf{s}_{sg}^{-1} \mathbf{h}_{sg}$ to find the side group energies and eigenstates. The corresponding side group orbitals for the C9 molecules responsible for the QI effects are plotted in Fig. 8.

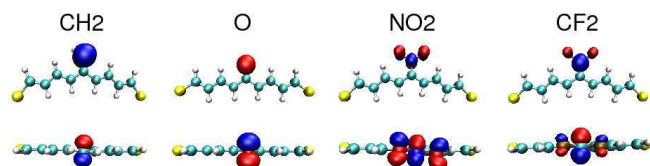


Fig. 8 Side group orbitals of C9 responsible for the QI effects close to the Fermi energy.

References

- R. Baer and D. Neuhauser, *J. Am. Chem. Soc.*, 2002, **124**, 4200–4201.
- E. H. van Dijk, D. J. T. Myles, M. H. van der Veen and J. C. Hummelen, *Org. Lett.*, 2006, **8**, 2333–2336.
- T. Markussen, J. Schiötz and K. S. Thygesen, *J. Chem. Phys.*, 2010, **132**, 224104.
- R. Stadler, S. Ami, M. Forshaw and C. Joachim, *Nanotechnology*, 2004, **15**, S115.
- R. Stadler, M. Forshaw and C. Joachim, *Nanotechnology*, 2003, **14**, 138.
- J. P. Bergfield and C. A. Stafford, *Nano Letters*, 2009, **9**, 3072–3076.
- C. M. Finch, V. M. Garcia-Suarez and C. J. Lambert, *Phys. Rev. B*, 2009, **79**, 033405–.
- J. P. Bergfield, M. A. Solis and C. A. Stafford, *ACS Nano*, 2010, **4**, 5314–5320.
- F. Sols, M. Macucci, U. Ravaioli and K. Hess, *Appl. Phys. Lett.*, 1989, **54**, 350–352.
- W. Porod, Z. Shao and C. S. Lent, *Appl. Phys. Lett.*, 1992, **61**, 1350–1352.
- W. Porod, Z. Shao and C. S. Lent, *Phys. Rev. B*, 1993, **48**, 8495–8498.
- P. Debray, O. E. Raichev, P. Vasilopoulos, M. Rahman, R. Perrin and W. C. Mitchell, *Phys. Rev. B*, 2000, **61**, 10950–10958.
- C. Patoux, C. Coudret, J. P. Launay, C. Joachim and A. Gourdon, *Inorg. Chem.*, 1997, **36**, 5037–5049.
- M. Mayor, H. B. Weber, J. Reichert, M. Elbing, C. von Hänisch, D. Beckmann and M. Fischer, *Angew. Chem. Int. Ed.*, 2003, **42**, 5834–5838.
- P. Sautet and C. Joachim, *Chem. Phys. Lett.*, 1988, **153**, 511–516.
- K. Yoshizawa, T. Tada and A. Staykov, *J. Am. Chem. Soc.*, 2008, **130**, 9406–9413.
- P. W. Fowler, B. T. Pickup, T. Z. Todorova and T. Pisanski, *J. Chem. Phys.*, 2009, **130**, 174708.
- T. Hansen, G. C. Solomon, D. Q. Andrews and M. A. Ratner, *J. Chem. Phys.*, 2009, **131**, 194704.
- D. Walter, D. Neuhauser and R. Baer, *Chem. Phys.*, 2004, **299**, 139–145.
- D. M. Cardamone, C. A. A. Stafford and S. Mazumdar, *Nano Lett.*, 2006, **6**, 2422–2426.
- C. A. Stafford, D. M. Cardamone and S. Mazumdar, *Nanotechnology*, 2007, **18**, 424014.
- S. H. Ke, W. Yang and H. U. Baranger, *Nano Lett.*, 2008, **8**, 3257–3261.
- M. H. Hettler, W. Wenzel, M. R. Wegewijs and H. Schoeller, *Phys. Rev. Lett.*, 2003, **90**, 076805.
- A. Donarini, G. Begemann and M. Grifoni, *Nano Lett.*, 2009, **9**, 2897–2902.
- R. Stadler, K. S. Thygesen and K. W. Jacobsen, *Nanotechnology*, 2005, **16**, S155–S160.
- T. A. Papadopoulos, I. M. Grace and C. J. Lambert, *Phys. Rev. B*, 2006, **74**, 193306.
- R. Stadler, *Phys. Rev. B*, 2009, **80**, 125401.
- G. C. Solomon, D. Q. Andrews, R. H. Goldsmith, T. Hansen, M. R. Wasielewski, R. P. Van Duyne and M. A. Ratner, *J. Am. Chem. Soc.*, 2008, **130**, 17301–17308.
- G. C. Solomon, D. Q. Andrews, R. H. Goldsmith, T. Hansen, M. R. Wasielewski, R. P. Van Duyne and M. A. Ratner, *J. Am. Chem. Soc.*, 2008, **130**, 17309–17319.
- T. Markussen, R. Stadler and K. S. Thygesen, *Nano Lett.*, 2010, **10**, 4260.
- A. E. Miroshnichenko, S. Flach and Y. S. Kivshar, *Rev. Mod. Phys.*, 2010, **82**, 2257.
- A. A. Clerk, X. Waintal, and P. W. Brouwer, *Phys. Rev. Lett.*, 2001, **86**, 4636.
- R. Stadler and T. Markussen, *submitted*.
- We calculate the electronic conductance of the molecular contacts using a well established combination of DFT and Green's function methods³⁶. The DFT and transport calculations are performed using the the real space projector augmented wave method GPAW³⁷ with the PBE exchange-correlation functional³⁸. We initially relax the molecule and the two closest Au layers using a double-zeta with polarization (DZP) atomic orbital basis set³⁹. For all the molecular junctions considered we find that the anchoring S atom prefers to bind to the Au(111) surface in a bridge site slightly shifted toward the hollow site. The transmission function of the relaxed junction is calculated using the DZP basis set following the standard DFT-Landauer approach described in e.g. Ref.⁴⁰.
- Since we have no electrode (Au) Fermi level in the TB calculations, we need to align the DFT calculations to the TB values. We choose to align the transmission peak corresponding to the LUMO since this is a very clear peak in all DFT and TB calculations. The DFT transmission node energies are thus rigidly shifted by $\Delta E = E_{\text{LUMO}}^{(\text{TB})} - E_{\text{LUMO}}^{(\text{DFT})}$.
- J. Enkovaara, C. Rostgaard, J. J. Mortensen, J. Chen, M. Dulak, L. Ferrighi, J. Gavnholt, C. Glinsvad, V. Haikola, H. A. Hansen, H. H. Kristoferssen, M. Kuisma, A. H. Larsen, L. Lehtovaara, M. Ljungberg, O. Lopez-Acevedo, P. G. Moses, J. Ojanen, T. Olsen, V. Petzold, N. A. Romero, J. Stausholm-Moller, M. Strange, G. A. Tritsarlis, M. Vanin, M. Walter, B. Hammer, H. Hakkinen, G. K. H. Madsen, R. M. Nieminen, J. K. Norkov, M. Puska, T. T. Rantala, J. Schiötz, K. S. Thygesen and K. W. Jacobsen, *J. Phys. Condens. Matter*, 2010, **22**, 253202.
- J. J. Mortensen, L. B. Hansen and K. W. Jacobsen, *Phys. Rev. B*, 2005, **71**, 035109.
- J. P. Perdew, K. Burke and M. Ernzerhof, *Phys. Rev. Lett.*, 1996, **77**, 3865.
- A. H. Larsen, M. Vanin, J. J. Mortensen, K. S. Thygesen and K. W. Jacobsen, *Phys. Rev. B*, 2009, **80**, 195112.
- M. Strange, I. S. Kristensen, K. S. Thygesen and K. W. Jacobsen, *J. Chem. Phys.*, 2008, **128**, 114714.